Image formation and restoration using multi-element synthetic array processing

Jeremy A. Johnson, Mustafa Karaman, Pierre Khuri-Yakub

Ginzton Laboratories, Stanford University, Stanford, CA, 94305

ABSTRACT

Traditionally, the number of transmit and receive processing channels is equal to the number of transducers (*N*) in an ultrasound imaging system. Certain applications limit the number of processing channels such that there are fewer channels than transducer elements. For these cases, a subset of *M* adjacent transducers—a multi-element subarray—performs echo transmission and reception. The processing channels are multiplexed across the array as beams are acquired from each of *K* subarrays. Combination of all subarray apertures creates a *multi-element synthetic aperture* (MSA) that represents the response of the entire system. Appropriate 1D filtering is applied in the spatial domain to restore a response approximating that of full phased array imaging. Compared to *full phased array* (FPA) imaging, MSA imaging reduces the number of front-end processing channels by a factor of *N*/*M*. Three variations of the method were simulated for a 128-element array using 32-element subarrays. The effects of the signal bandwidth, subsampling rate, and filter length on the reconstructed 2D point-spread functions are shown. The method closely approximates the performance of FPA imaging with fewer processing channels.

Keywords: synthetic aperture, phased subarray, ultrasound, multi-element synthetic aperture

1. INTRODUCTION

Current ultrasound systems employ highly parallel hardware architecture for acoustic transduction, amplification, filtering, time-gain compensation, and digital-to-analog conversion. For each of the *N* transducer elements, *N* dedicated transmit and receive hardware channels are required that process the signals between the beamformer and the transducers in both directions. The hardware required for this architecture is both costly and bulky. This is especially true when the transducers and the beamforming hardware are physically separated, requiring *N* shielded coaxial cables to connect the two units. Mainstream systems typically use 128 or more transducer elements and the parallel hardware to support them. As the number of transducer elements increases, it becomes impractical to employ parallel transmit and receive processing channels for every array element.[1] This is especially true for 2D transducer arrays for 3D image acquisition, where a relatively small 16×16-element array requires 256 parallel channels.

Full-phased array (FPA) imaging, the most common beamforming method, requires parallel transmit and receive processing hardware since all elements simultaneously transmit and receive when forming a scanline.[2-4] The use of sparse arrays has been a common approach to reduce the number of parallel channels. Although the number of processing channels is successfully reduced, the number of transducer elements is reduced as well. In addition, the point-spread function (PSF) obtained by using sparse arrays suffers from high side lobe levels.

We present a solution that reduces the number of parallel processing that still uses all transducers, but only transmits and receives on a subset of the elements—a *subarray*—at any given time. This paper presents a solution that uses a novel beamforming method to synthesize an effective aperture from the effective subarray apertures. The beamforming method is referred to here as multi-element synthetic aperture (MSA).[5, 6]

The number of parallel processing channels required for this method is equal to *M*, the number of elements in each subarray. Multiplexing hardware can be used to select the active subarray, allowing the *M* parallel channels to be time-multiplexed such that all *N* elements are used. A subset of the beamlines is acquired by each subarray sequentially for each image frame. A final full resolution image can be reconstructed by using the proper number of acquired beams from each subarray. Image reconstruction involves beam upsampling and 1D reconstruction filtering of each subarray image. The reconstructed beams are coherently summed to form the final full resolution image.

Medical Imaging 2002: Ultrasonic Imaging and Signal Processing, Michael F. Insana,
William F. Walker, Editors, Proceedings of SPIE Vol. 4687 (2002) © 2002 SPIE · 1605-7422/02/$15.00

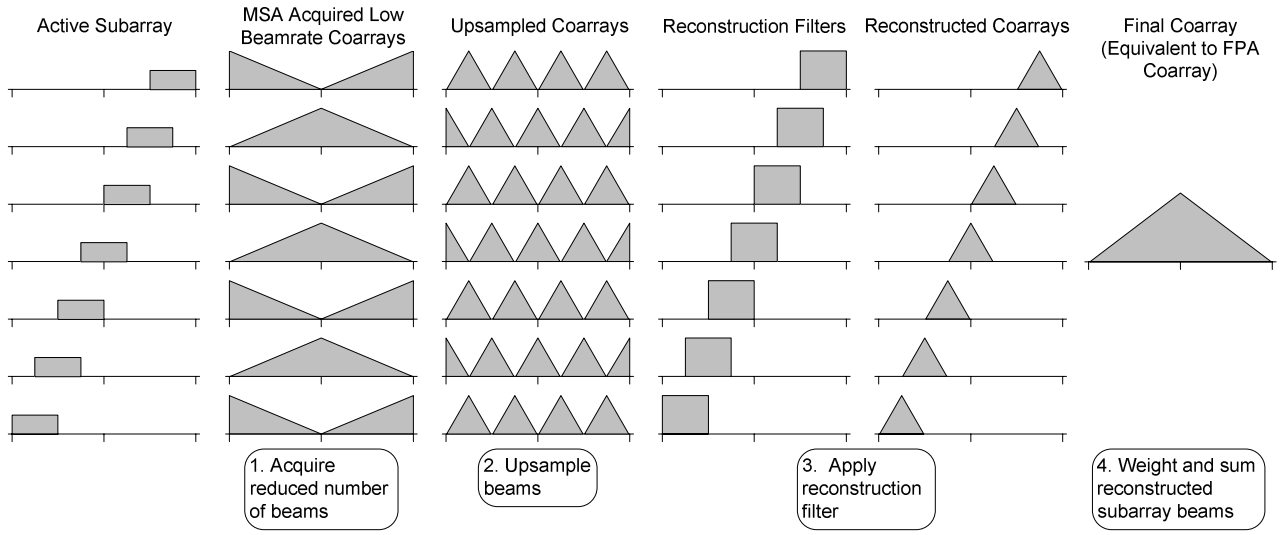

Figure 1. Coarray responses at each stage of the multi-element synthetic aperture (MSA) image formation algorithm. Ideally, the reconstructed coarrays will equal the coarray that would be obtained from each subarray if full beamrate samples were acquired. The resulting coarray is equivalent to that of the FPA imaging method.

2. METHODS

2.1 Aperture function and coarray definitions

The aperture function, PSF, and coarray function are used to design and evaluate the performance of a coherent array imaging system, and are all interrelated. The coarray function—also known as the effective aperture function—represents the lateral spatial frequency response of the array in the far field (the Fraunhofer region).[7, 8] The coarray function is given by

$$u[n] = a_t[n] \otimes a_r[n], \tag{1}$$

where $\otimes$ is the convolution operator, and $a_t[n]$ and $a_r[n]$ are the transmit (TX) and receive (RX) aperture functions, respectively.

For a continuous-wave (CW) system, the lateral PSF is approximated by the Fourier transform of the coarray function:

$$U[q] = \Im\{u[n]\} = \Im\{a_t[n]\} \cdot \Im\{a_r[n]\}. \tag{2}$$

This PSF represents the roundtrip response of a coherent array imaging system to a single point reflector in the far field.[9] While the relationship is derived for CW excitation, it remains useful when designing narrow bandwidth systems. The PSF roughly characterizes the performance of the imaging system. An ideal PSF has a narrow main lobe and minimal energy outside the main lobe.

The active subarrays and reconstructed coarrays shown in Figure 1 illustrate typical subaperture and corresponding coarrays, respectively.

2.2 Subarray representation

For subarray acquisition, each of the K subarrays has a corresponding aperture function. The k^{th} transmit and receive aperture functions are denoted as $a_{k_t}[n]$, and $a_{k_r}[n]$, respectively. Each subarray can be written in terms of a reference subarray, $a_0[n]$, located at the end of the array and the subarray spacing, P:

$$a_k[n] = a_0[n - kP],\ k = 0 \ldots K\text{-}1. \tag{3}$$

Equation 4 is true for both transmit and receive subarrays, and thus the index k can represent either the transmit subarray index, k_t, or the receive subarray index, k_r. A subarray spacing, P, equal to M represents adjacent non-overlapping subarrays. Similarly, if $u_0[n]$ is the cosubarray corresponding to a transmit and receive aperture function $a_0[n]$, then the cosubarray function corresponding to any transmit and receive subaperture is given by

$$u_{k_t,k_r}[n] = u_0[n - (k_t + k_r)P] \tag{4}$$

and the PSF for this combination of subarrays is

$$U_{k_t,k_r}[q] = U_0[q] \cdot \exp(-j(k_t + k_r)Pq). \tag{5}$$

Note that the same response can be obtained by different combinations of subarrays. For instance, transmitting on the second subarray ($k_t = 2$) and receiving on the third subarray ($k_r = 3$) is equivalent to transmitting on the fourth subarray ($k_t = 4$) and receiving on the first ($k_r = 1$). The resultant coarray and system PSF without any restoration is the sum of the individual cosubarrays and PSFs:

$$u[n] = \sum_{k_t} \sum_{k_r} u_0[n - (k_t + k_r)P], \tag{6}$$

and

$$U[q] = U_0[q] \cdot \sum_{k_t} \sum_{k_r} \exp(-j(k_t + k_r)Pq) \tag{7}$$

If $P = M$, then the subarray responses can simply be weighted and summed such that the final PSF and coarray function are equivalent to those of a full phased array system. In other words, the subarray restoration filters are all-pass with different gains. For any other choice of P, however, a frequency-shaping restoration filter must be applied on either the subarray beams or the reconstructed beams.

An easy method for visualizing the relationship between the subarray TX/RX combination and the coarray response is shown in Figure 2. The subarray/coarray relationship is diagrammed for three different beam acquisition and reconstruction methods. The diamond-shaped box at the top of each method indicates which TX and RX combinations are used for each method. One block in the diamond represents a single TX/RX combination. Each of these combinations forms a coarray that, when combined with all the other combinations, synthesizes a complete system coarray. As previously mentioned, there are different combinations of TX and RX subarrays that contribute identical coarrays. These particular combinations are easily visualized in this diagram as they are vertically aligned with one another. The first imaging method shown in Figure 2 acquires beams from all combinations of TX and RX elements. The resulting synthesized coarray is triangular, exactly equal to the coarray result from FPA imaging using all N elements simultaneously. This method is referred to as MSA-Full (MSA-F).

The other two methods use a *partial* set (MSA-P) and a *minimal* set (MSA-M) of TX/RX subarray combinations, each further reducing the number of redundant coarrays. Each combination requires a set of beam acquisitions, thus reducing these redundant combinations corresponds to an increased frame rate. MSA-P eliminates redundant combinations using the same set of coarrays and weighting the responses from each combination appropriately prior to coherent summation to reconstruct the FPA-equivalent coarray. MSA-M actually uses $2N/M - 1$ subarrays rather than N/M (seven instead of four for the example in Figure 2 and $P = M/2$. Although this slightly complicates the multiplexing hardware, the number of parallel channels is still reduced, and the number of beam acquisitions is minimized. It may first appear that the same minimum number of beam acquisitions would be possible using only N/M subarrays by selecting the four combinations along the diagonal and three just above the diagonal. However, it turns out that the phase from subarray combinations using $k_t = k_1$ and $k_r = k_2$ must be compensated by obtaining the opposite combination, $k_t = k_2$ and $k_r = k_1$, to avoid unnecessary distortion.

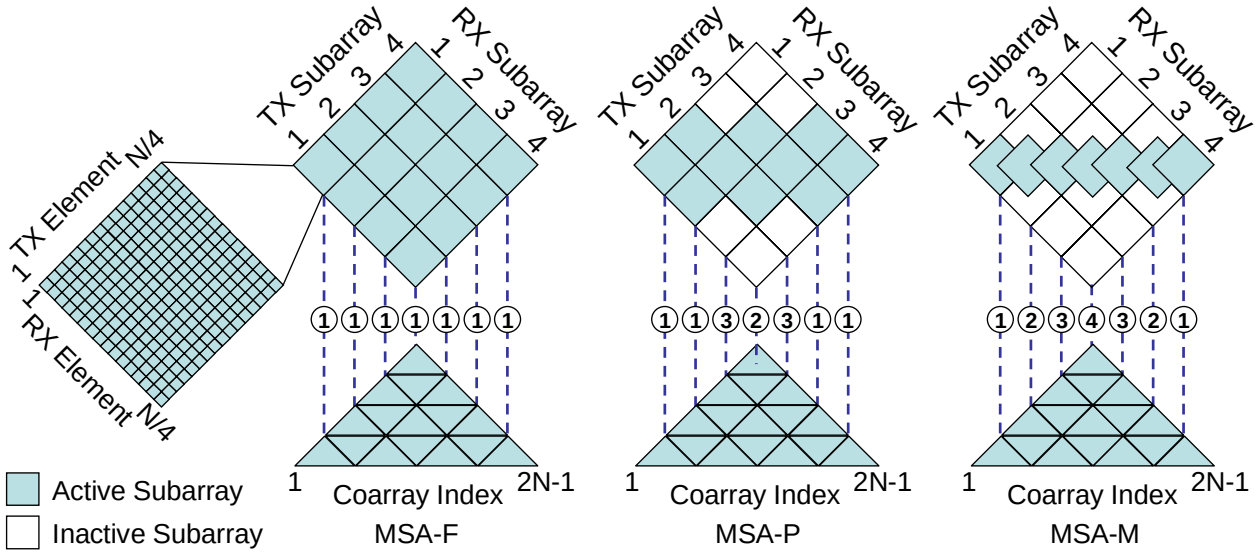

Figure 2. Coarray representation of three different multi-element synthetic aperture image reconstruction methods. Each TX and RX subarray combination contributes to different lateral spatial frequencies represented by the coarray. Weighting and summing of the subarray responses approximates the coarray of conventional full-phased array (FPA) imaging.

2.3 Beamspace sampling

Only a subset of the beams that would be acquired for FPA imaging are acquired by each subarray combination. The subarray beam acquisition steps for MSA-M are shown in Figure 3. Beam acquisition is similar for MSA-F and MSA-P, except that each beam is sampled by every subarray combination, not just for $k_t = k_r$.

$$Q \geq 2(2N-1)\frac{d}{\lambda}\sin\left(\frac{\Theta}{2}\right), \tag{8}$$

where d is the array element pitch, λ is the acoustic wavelength, and Θ is the scan angle. Since the number of beams must be an integer, Q is typically chosen to be the next largest integer that satisfies the inequality. In general, $d = \lambda/2$, in which case the sampling criteria simplifies to

$$Q \geq (2N-1)\sin\left(\frac{\Theta}{2}\right). \tag{9}$$

Each subarray acts as an independent phased array, and thus has its own sampling requirement:

$$Q^S \geq (2M-1)\sin\left(\frac{\Theta}{2}\right) \tag{10}$$

Typically $M \ll N$, therefore each subarray acquires $Q^S \ll Q$ beams. The total number of firings required for a given frame is

$$F = Q^S K, \tag{11}$$

where K is the total number of subarray combinations used.

2.4 Upsampling, reconstruction, and restoration

The final image must have a sufficient number of beams to meet the beam sampling criteria for the full array. Accordingly, the subarray beams are upsampled by inserting an integer number of zero-valued beams between acquired

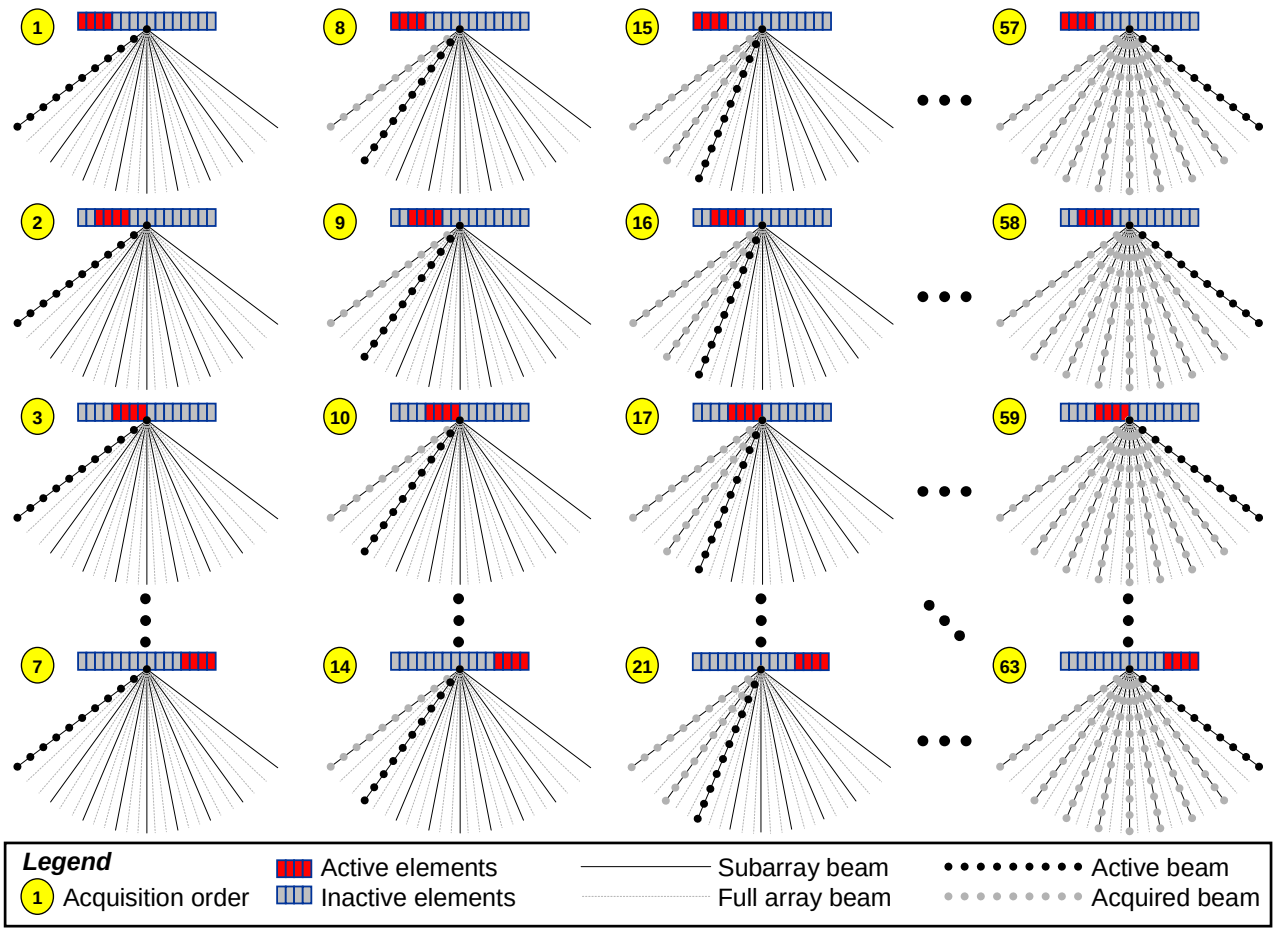

Figure 3. Subarray beam acquisition steps. Each subarray is used to acquire a subset of the beams that would normally be acquired for FPA imaging. This subset of beams forms a low beamrate image. All subarrays sample the same beam sequentially in order to reduce motion artifacts.

beams. The amount of upsampling can be expressed in terms of Q^S, the number of subarray beams, and Q, the number of final beams:

$$L \le \frac{Q}{Q^S} \tag{12}$$

Acquiring fewer than N beams during a subarray beam acquisition corresponds to downsampling of the PSF and cyclical expansion of the coarray. If Eq. 12 is not satisfied, the coarray can wrap around onto itself, causing aliasing. Figure 1 demonstrates the result of critically-sampled beams such that the nonzero portion of the coarray stretches to occupy all of coarray space. Likewise, lateral upsampling in beam space corresponds to contraction and periodic replication in co-array space. The coarray of the upsampled beams is also shown in Figure 1.

Prior to combining the results of each subarray, a reconstruction filter with a pass-band matching the cosubarray functions must be applied across the upsampled subarray beams to avoid aliasing in the final image. The coarray representation of ideal pass-band filters is shown in Figure 1. Unless all subarray combinations are acquired—such as in MSA-F processing—a restoration filter is required to restore the overall response to match that of FPA imaging. The restoration required is a simply a scaling of each subarray combination, and can be applied as an all-pass filter with constant gain.

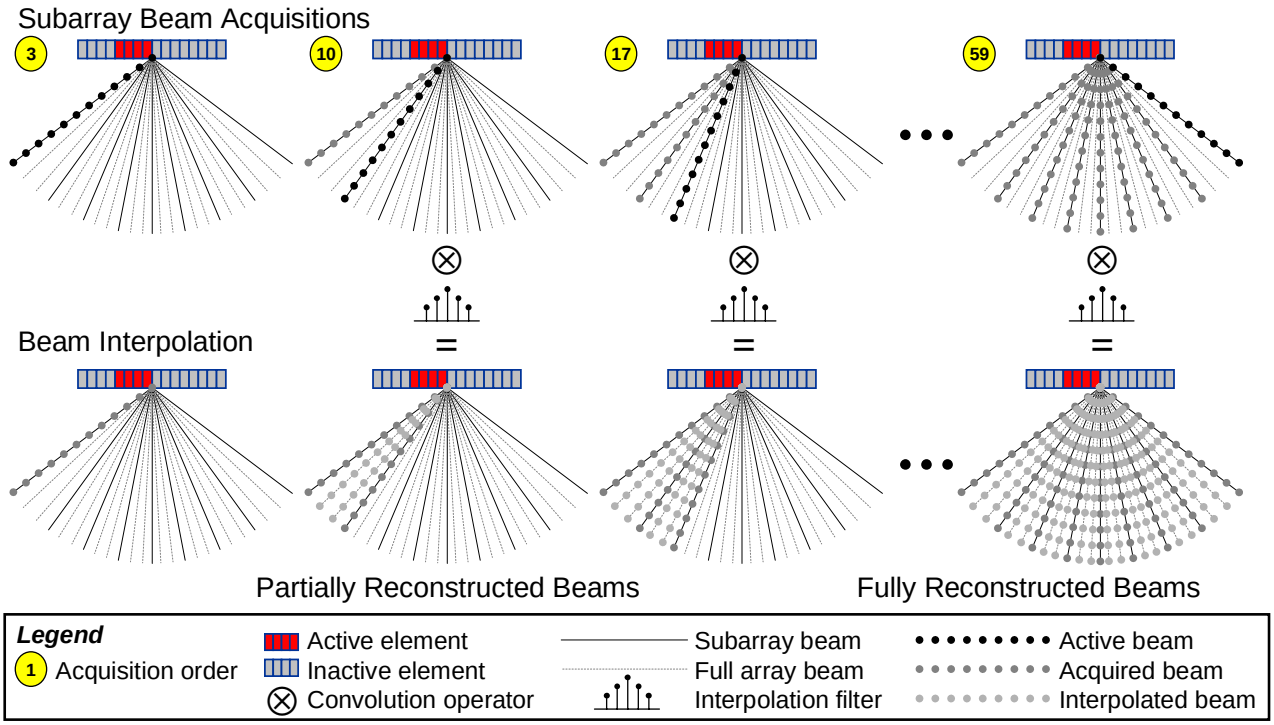

Figure 4. Beam interpolation. As the low beamrate beams are being acquired, interpolation filters reconstruct the remaining beams which will form the high beamrate image.

The reconstruction filter can be applied while the beams are being acquired. Figure 4 illustrates how the (unacquired) high beamrate beams are reconstructed using acquired beams from each subarray.

2.5 Beamforming and image reconstruction simulations

In order to test the performance of the algorithm and to compare it to traditional FPA imaging, all the methods were used to reconstruct an image of a single point target from simulated A-scans. Testing the beamforming methods on simulated A-scans provides a controlled, noise-free environment in which differences in resulting PSFs can confidently be attributed to differing performances of the beamforming method.

The pulses used for the simulations were Gaussians of differing variance modulated at a center frequency, f_0, of 3 MHz. The 1D transducer array has 128 elements with an element pitch, d, equal to $\lambda/2$. A single perfect point reflector was placed at a distance of 3.444 apertures ($f^{\#}$) from the array in the center of the imaging field. The A-scans are sampled at $32f_0$.

Four beamforming methods are used: FPA, MSA-M, MSA-P, and MSA-F. For each method, the final beamset consists of 511 beams with a scan angle of 180°. FPA imaging acquires all 511 beams sequentially to form the final image. For both FPA and MSA, transmit beamforming has a fixed focus at the distance of the point reflector, while receive beamforming focuses dynamically. Beams are sampled at a rate of $4f_0$.

The MSA methods each used 32-element subarrays. The transmit and receive focusing delays used for beam steering and focusing are the same for each of the 32 elements as they would be if they were acting as part of the full array for FPA imaging. For each of the subarray combinations, $Q^S = Q/L$ beams are acquired that span 180° and are evenly spaced in $\sin\theta$. L is referred to as the beam subsampling rate. The beams are upsampled by inserting $L - 1$ zero-valued beams between each of the subarray beams. Ideal pass-band filters corresponding to each unique coarray contribution

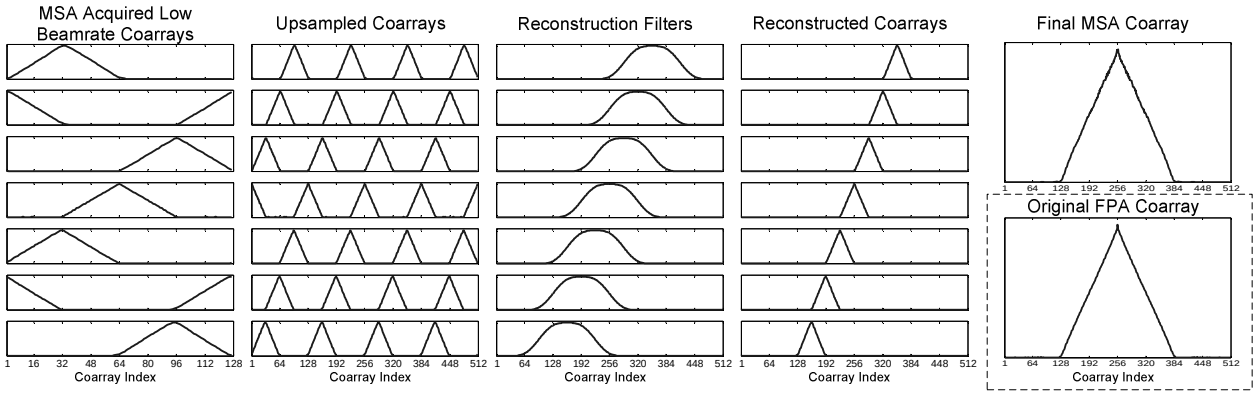

Figure 5. MSA-M processing simulation results. The coarrays for each stage of the MSA-M process are shown for simulated beams. The simulation used a 5% bandwidth Gaussian pulse, a 128-element subarray, seven overlapping 32-element subarrays, a subsampling rate of 4, and a 31-tap reconstruction filter ($N = 128$, $M = 32$, $L = 4$). A Hamming window was applied to the ideal bandpass reconstruction filter. The reconstructed beams were weighted and summed to form the final MSA image. These results closely match the theoretical results because the low bandwidth pulse is similar to continuous-wave excitation for which the Fraunhofer approximation is derived.

are calculated and truncated to the desired length, and a Hamming window function is applied. The appropriate filters are laterally convolved with the upsampled beams, then coherently summed prior to envelope detection and logarithmic compression for proper display.

3. RESULTS

The theory used to justify the MSA method was based on the 1D lateral PSF and coarray response to a CW imaging system. Figure 5 shows how closely the simulations match the theoretical model given in Figure 1. There are two differences between these results and the model. First, the subsampling rate is not at the critical limit, but is twice this limit. This causes the nonzero portion of the acquired low beamrate coarrays to extend over half the coarray range. As a result, the replicates of the response in the upsampled coarrays are spaced sufficiently apart such that the reconstruction filter does not overlap with undesired adjacent replicates. The second difference between the results and the model is that a Hamming window is applied to the filter kernel in beamspace, resulting in a smoother coarray response. The smoother coarray response reduces the moment of the filter kernel, allowing the kernel to have a shorter length. The results were obtained using a 5% bandwidth Gaussian pulse, as a lower bandwidth pulse more closely approximates the response of CW imaging.

In order to study the effect of different bandwidth signals, all four beamforming methods were applied to A-scans formed using differing signal bandwidths. The 2D PSFs for five of these bandwidths and for all beamforming methods are shown in Figure 6. As expected, the longer pulses corresponding to a narrower bandwidth resulted in a PSF with a larger axial main lobe width. While the 3 dB lateral resolution for all bandwidths and beamforming methods remains constant at 0.90°, the 3 dB axial resolution varies with bandwidth (Figure 8).

More interesting is how the PSFs of the three MSA methods differ from that of FPA imaging, since this is considered to be the best that can be done if all elements are used to acquire each beam. As shown in Figure 7, the lateral PSF for all MSA methods are in excellent agreement with the PSF for FPA. While these were expected to perform well along the focal line, it was uncertain how well the 2D PSFs would agree with the FPA PSFs. The “arms” of the PSF seem to be reasonably well reconstructed. The primary weakness appears between these arms. This is primarily due to the PSFs of the low beamrate subarray images are not aligned. The reconstruction filter transfers these misaligned PSF arms into otherwise blank regions. This effect increases with increasing bandwidth as the system becomes less and less like a CW system. Note the similarity between all MSA PSFs. If the simulations included electronic noise, the MSA method with more subarray combinations would have a higher SNR.

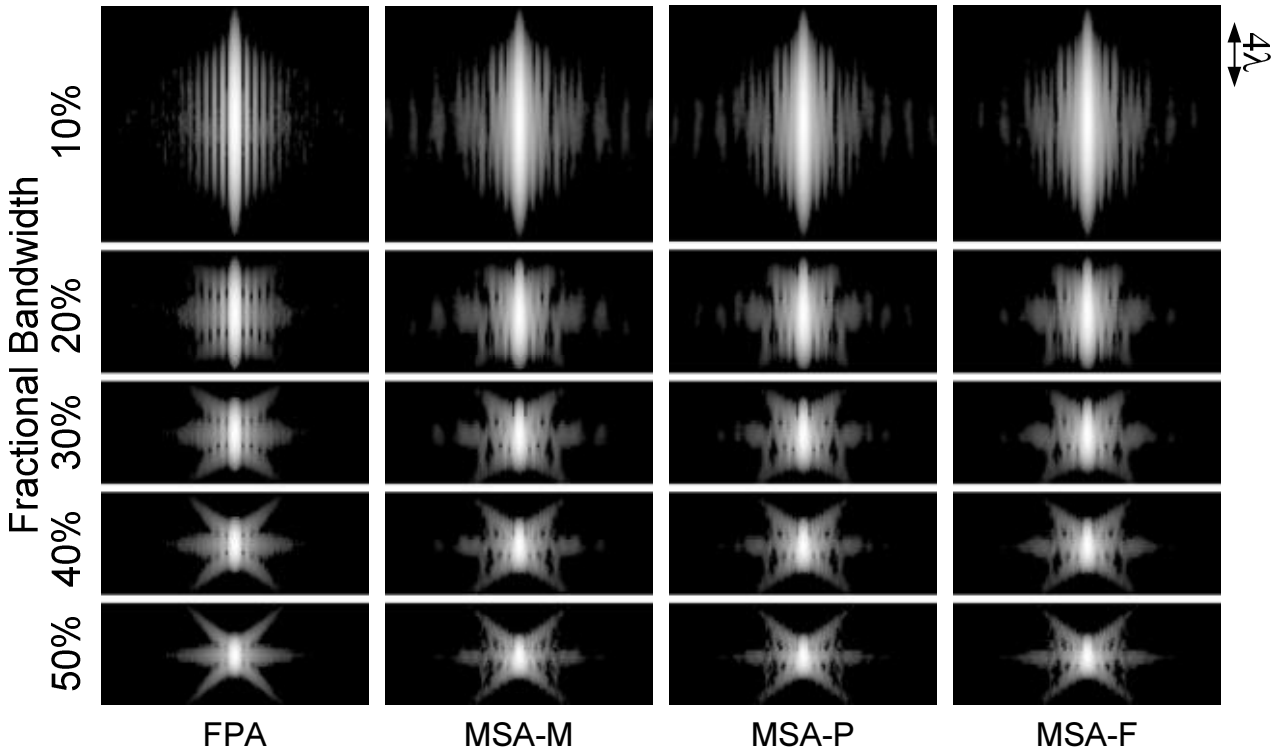

Figure 6. 2D PSF results at varying signal bandwidths. Simulation results showing the how the pulse bandwidth affects the PSF. The responses of all MSA imaging methods have imperceptible differences. Their responses can be compared to the best PSF obtained by from using FPA imaging. Each PSF is 30° wide, evenly spaced in $\sin\theta$, and displayed with 60 dB of logarithmic compression.

The effect of the beam subsampling rate on the PSF can be observed in Figure 9(a). For these images, the filter length scaled with the subsampling rate such that a constant number of acquired beams (eight in this case) contributed to any reconstructed beam. In this case, the critical sampling rate is 8. It may be concluded that when using MSA beamforming, the quality is not significantly degraded if the beamsampling rate is at least twice the Nyquist rate.

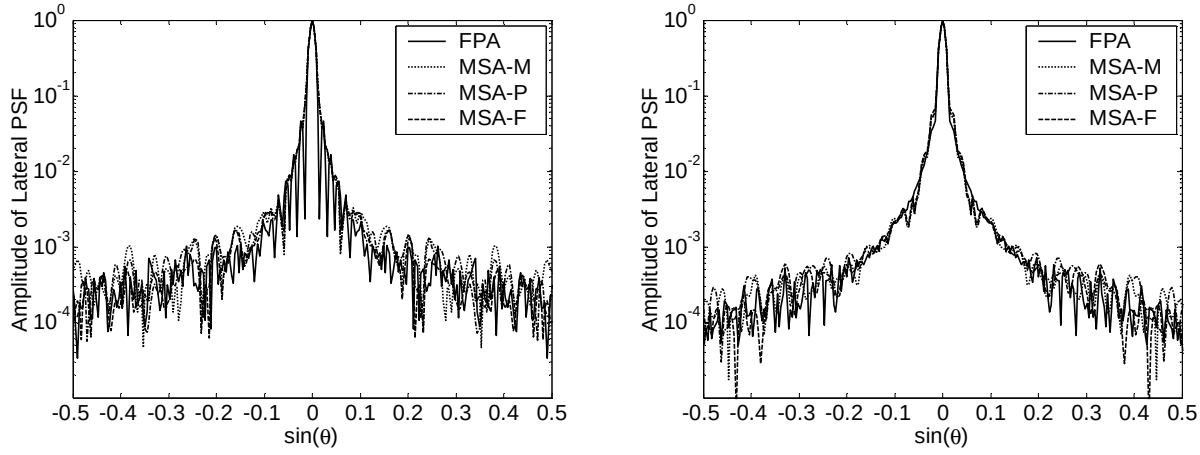

Figure 7. 1D lateral PSFs for 10% and 50% bandwidth. The 3 dB lateral resolution for all image reconstruction methods is 0.90°.

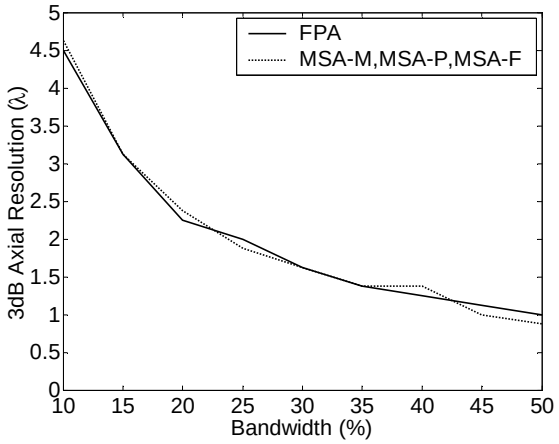

Figure 8. 3 dB axial resolution dependence on signal bandwidth. As expected, wider bandwidth pulses correspond to lower axial resolutions. The resolution obtained from all MSA methods closely approximates that of conventional FPA imaging.

Because imaging differences between the MSA methods are imperceptible, only the PSFs for MSA-M are shown.

The last results, shown in Figure 9(b), demonstrate the effect of using a fixed subsampling rate and filters of different lengths. Although the PSFs take on unique forms, the lateral and axial resolutions remain fixed, and it is not clear that a significant improvement is occurring with increasing filter length.

4. CONCLUSION

MSA imaging is an effective method to significantly reducing the number of parallel processing channels with only a slight degradation in quality compared to FPA imaging. For a 128-element array with 32 parallel processing channels, 7 subarray combinations can be used to acquire 128 beams each, and a 31-tap filter can be applied to reconstruct a reasonable image. As compared to FPA imaging, this setup represents a frame rate decrease by 43% and a hardware complexity reduction of 75%.

There are several potential methods for improving MSA reconstruction methods. First, 2D filter kernels designed for each subarray combination could be used. The results shown here apply 1D filter kernels in the lateral direction. The 1D array only achieves near-perfect reconstruction at the focal point, and a 2D filter would better compensate for the 2D nature of the PSF. With the added improvement of a 2D filter would come additional hardware necessary to perform 2D convolution; further investigation is required to study this tradeoff.

One way to potentially improve the frame rate of MSA imaging is to reduce the number of subarrays used for the MSA-M method, in turn increasing the subarray distance *P*. Currently, all-pass constant gain filters can restore an FPA-equivalent response from the coherent sum of the MSA-M subarray responses. A reduced overlap of the subarray coarrays would result in a non-uniform total coarray response. Using a more sophisticated restoration filtering scheme, this may lead to further improvement of frame rate with no increase in hardware complexity.

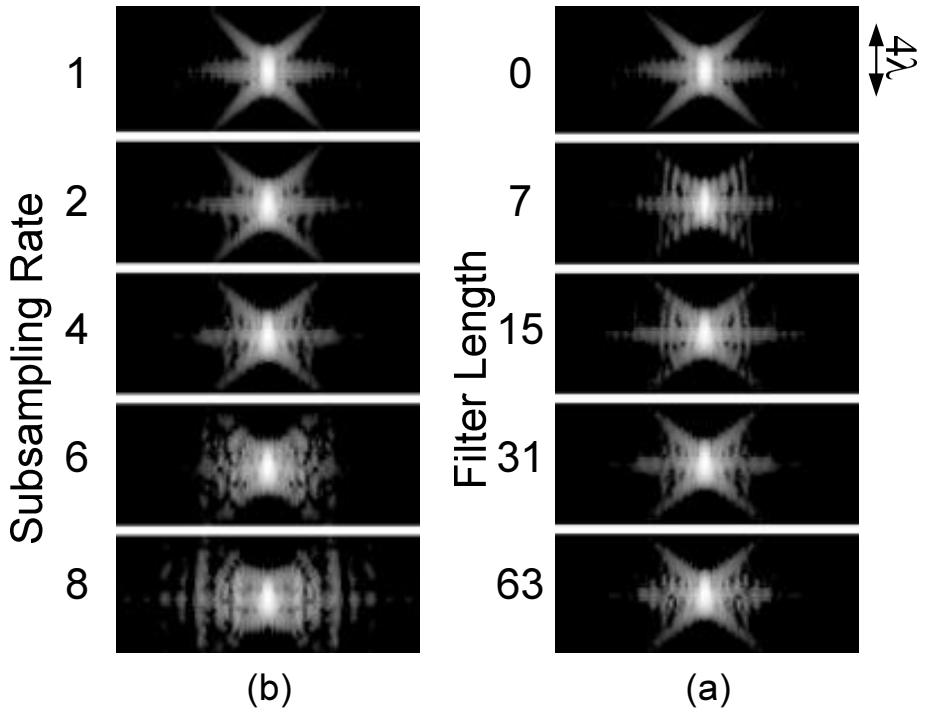

Figure 9. (a) PSF dependence on subsampling rate. The filter length varies such that each beam is reconstructed using four acquired beams. (b) PSF dependence filter length. A subsampling rate of 4 is used, and filters of varying lengths are used to reconstruct the PSFs. All PSFs shown were formed using MSA-M, but MSA-P and MSA-F are equivalent and have imperceptible differences.

REFERENCES

1. M. E. Schafer and P. A. Lewin, "The influence of front-end hardware on digital ultrasonic imaging," *IEEE Transactions on Sonics and Ultrasonics*, pp. 295-306, 1984.
2. B. D. Steinberg, *Principles of Aperture and Array System Design : Including Random and Adaptive Arrays*. Wiley, New York, 1976.
3. B. A. J. Angelsen, *Ultrasound Imaging, Vol. 1*. Emantec, Trondheim, 2000.
4. T. A. Shoup and J. Hart, "Ultrasonic imaging systems," *Proceedings of the IEEE 1988 Ultrasonics Symposium*, **2**, pp. 863-71, IEEE, New York, 1988.
5. M. Karaman, "Ultrasonic array imaging based on spatial interpolation," *Proceedings of the 3rd IEEE International Conference on Image Processing*, **1**, pp. 745-8, IEEE, New York, 1996.
6. M. Karaman and M. O'Donnell, "Subaperture processing for ultrasonic imaging," *IEEE Transactions on Ultrasonics, Ferroelectrics and Frequency Control*, **45**, pp. 126-35, 1998.
7. R. T. Hoctor and S. A. Kassam, "The unifying role of the coarray in aperture synthesis for coherent and incoherent imaging," *Proceedings of the IEEE*, **78**, pp. 735-52, 1990.
8. R. J. Kozick and S. A. Kassam, "Synthetic aperture pulse-echo imaging with rectangular boundary arrays (acoustic imaging)," *IEEE Transactions on Image Processing*, **2**, pp. 68-79, 1993.
9. J. W. Goodman, *Introduction to Fourier optics*. McGraw-Hill, San Francisco, 1968.